JTTEE5 4:401-407

Formation of Structure of WC-Co Coatings on Aluminum Alloy Substrate During High-Velocity Oxygen-Fuel (HVOF) Spraying

V.V. Sobolev, J.M. Guilemany, and J.A. Calero

This paper is based on Ref 1 and concerns the mathematical simulation of the structure formation of the WC-Co coating on aluminum alloy (Al-4% Cu) substrate during high-velocity oxygen-fuel (HVOF) spraying. Variations of the solidification velocity, thermal gradient, and cooling velocity in the coating and substrate interfacial region are studied. Formation of the amorphous and crystalline structures in the coating and of the crystalline structure in the substrate interfacial region is discussed. Behavior of the crystal size and intercrystalline distance with respect to the thermal spray parameters is analyzed. Optimal conditions for the development of fine and dense crystalline structure are established. Results agree well with experimental data.

1. Introduction

PROPERTIES of thermal spray coatings essentially depend on the coating structure formed during solidification (Ref 2-5). Structure formation processes depend on the thermophysical properties of the substrate and coating. In Ref 3 to 5, structural characteristics of the WC-Co and WC-Ni coatings, which were HVOF sprayed on to a low-carbon steel, were studied.

This article investigates coating structure development during HVOF spraying of agglomerated powder particles, consisting of WC in a Co-40%W alloy binder, on to an aluminum (Al-4%Cu) substrate. The analysis is a mathematical simulation based on the model described in Ref 6 and on the results of the thermal calculations given in Ref 1. Special attention is paid to structure formation in the first coating layer and the substrate interfacial zone because they comprise the region where the substrate-coating adhesion and bonds are developed. The results agree well with the experimental data. They also aid in the investigation of the formation of coating defects, such as gas and shrinkage porosity, using the methods described in Ref 7 and 8.

In the basic mathematical simulation, the following parameters were fixed (Ref 1). The substrate thickness is 3 mm. The coating layer thickness, δ, is 15 μm. The substrate initial temperature, T_{10} is 20 °C. The heat transfer coefficient at the upper surface of a coating layer, α, is 1000 $Wm^{-2}K^{-1}$. The contact heat transfer coefficient at the substrate-coating interface, α_{c1} is 4×10^6 $Wm^{-2}K^{-1}$, and the coefficient between the subsequent layers, α_{c2}, is 1.3×10^6 $Wm^{-2}K^{-1}$. The fluid temperature near a coating layer upper surface, T_b, is 500 °C. The tungsten volume fraction in the metallic matrix alloy is 0.52. The metallic phase volume fraction is 0.68. The time between application of different coating layers is 1.325 (Ref 1).

Keywords HVOF processing, interfacial zone, prediction of microstructures; solidification modeling

V.V. Sobolev, J.M. Guilemany, and **J.A. Calero,** Metalurgia Física-Ciencia de Materiales, Departamento de Ingeniería Química y Metalurgia, Universidad de Barcelona, Martí y Franqués, 1, 08028, Barcelona. Spain.

2. Coating First Layer

2.1 *Solidification Isotherms*

The main heat removal from the first coating layer occurs because the substrate is a heat sink. Therefore, layer solidification starts from the substrate-coating interface (Ref 1, 3-6). Because the upper layer surface is cooled by the surrounding gases, there is generally an additional solidification front moving from this surface toward the interface. But this solidification process may be neglected in comparison with that caused by heat transfer to the substrate (Ref 1, 6), particularly in the case of the aluminum alloy substrate.

Due to the WC dissolution in-flight, a Co-W-C alloy phase is formed. As its carbon content is negligible, this alloy may be considered as a Co-W binary alloy with high tungsten content. Alloy solidification depends on the movement of the surfaces at the liquidus temperature, T_{L2}, and solidus temperature, T_{S2}, which bound the solid-liquid (mushy) zone region.

As the first layer cools, the liquidus isotherm appears near the interface. Isotherm velocity, v_{L2}, is initially very high and then diminishes abruptly as the solidification latent heat is extracted. The solidus isotherm moves with the velocity, v_{S2}, at first rapidly and then more slowly due to latent heat extraction.

The thermal gradients, G_{L2} and G_{S2}, at the liquidus and solidus, respectively, are steep near the substrate-coating interface. Then they decrease, at first rapidly and afterward more slowly, when the heat removal becomes competitive with the extraction of latent heat.

Both cooling velocities, v_{CL2} and v_{CS2}, at the liquidus and solidus, respectively, diminish sharply near the interface and then vary more slowly.

Mean values of the parameters of the solidification isotherms were also calculated with respect to time. Behavior at the liquidus and solidus follows a similar pattern. Behavior at the solidus is discussed here.

Mean solidification velocity, v_{S2}, decreases with layer thickness and varies nonuniformly with initial layer temperature (Fig. 1). The mean cooling velocity, v_{CS2}, also diminishes with δ (Fig. 2) and varies nonuniformly with the layer initial temperature T_{20}.

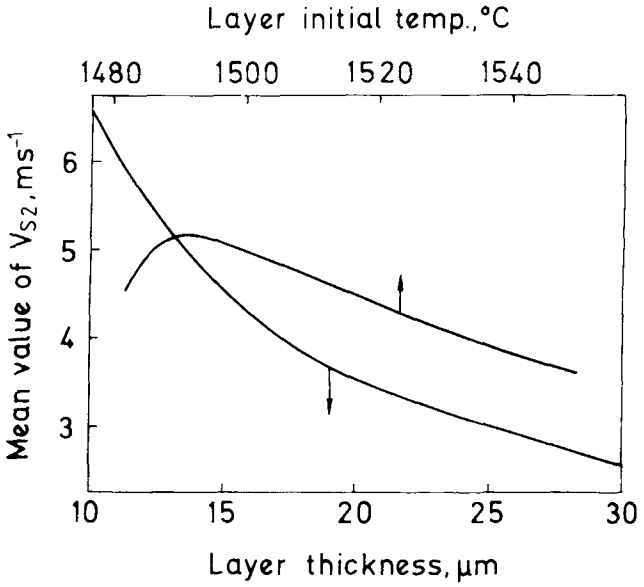

Fig. 1 Variations of mean values of solidification velocity, v_{S2}, with respect to layer thickness and initial temperature

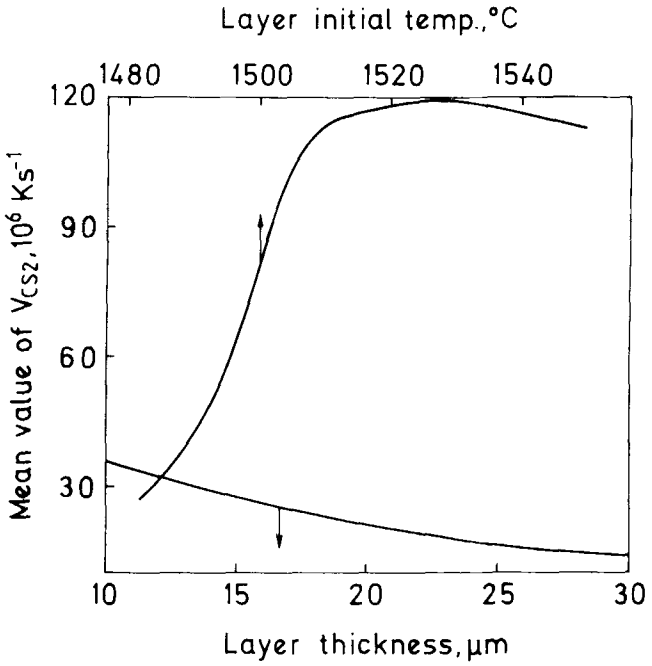

Fig. 2 Variations of mean values of cooling velocity, v_{CS2}, with respect to layer thickness and initial temperature

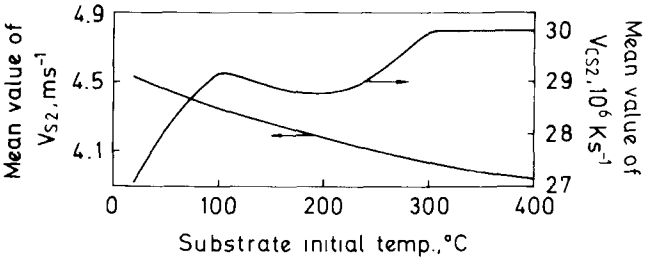

Fig. 3 Variations of mean values of solidification velocity, v_{S2}, and cooling velocity, v_{CS2}, with respect to substrate initial temperature

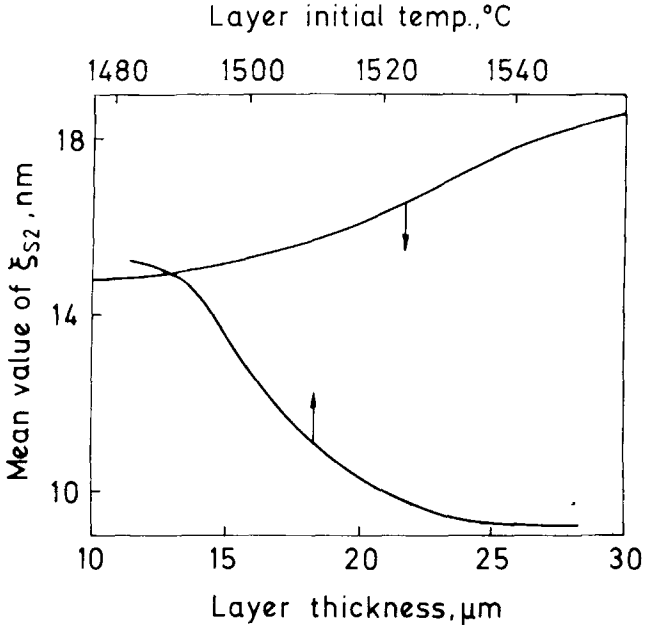

Fig. 4 Variations of mean values of crystal size, ξ_{S2}, with respect to layer thickness and initial temperature

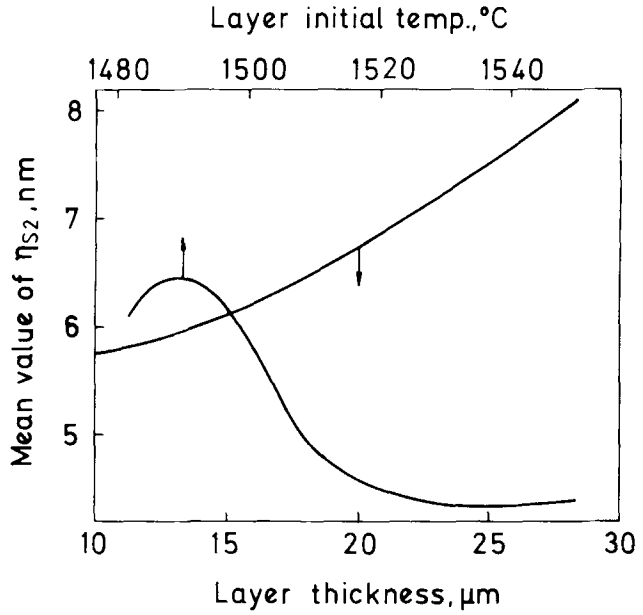

Fig. 5 Variations of mean values of intercrystalline distance, η_{S2}, with respect to layer thickness and initial temperature

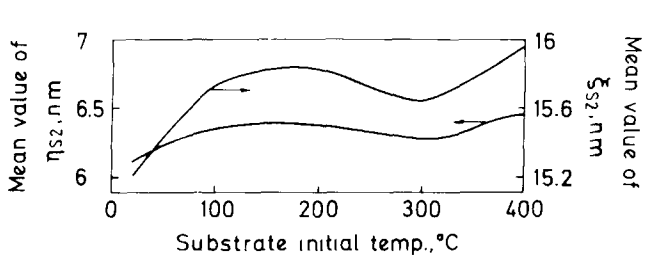

Fig. 6 Variations of mean values of crystal size, ξ_{S2}, and intercrystalline distance, η_{S2}, with respect to substrate initial temperature

This nonuniform behavior results from the competition between heat removal and heat accumulation. At first, the increase of the initial layer temperature causes thermal gradients between the layer and the substrate to grow and heat removal from the layer to accelerate. As a result, the mean values of both v_{S2} and v_{CS2} at first rise with T_{20}. The further increase of T_{20} leads to the marked accumulation of heat in the first coating layer, which begins to prevail over the growth of the thermal gradients, causing the mean values of v_{S2} and v_{CS2} to decrease.

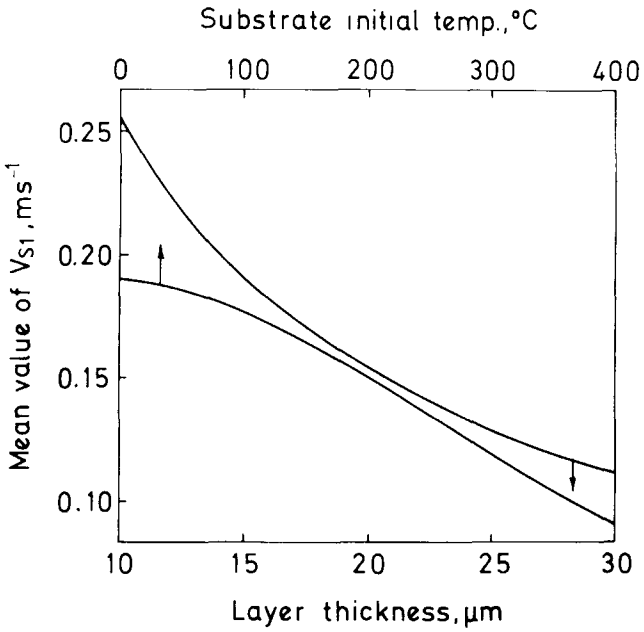

Fig. 7 Variations of mean values of solidification velocity, v_{S1}, with respect to layer thickness and substrate initial temperature

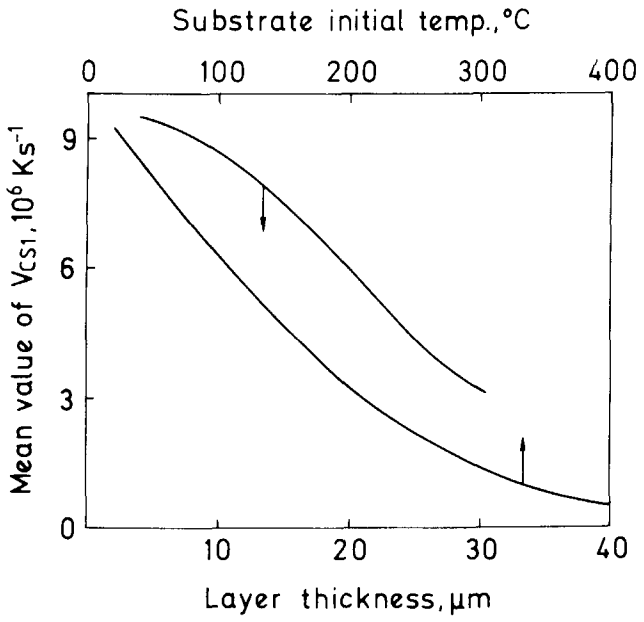

Fig. 8 Variations of mean values of cooling velocity, v_{CS1}, with respect to layer thickness and substrate initial temperature

Figure 3 shows that the mean values of v_{S2} diminish with the initial substrate temperature while the mean values of v_{CS2} vary nonuniformly with respect to T_{10}. The mean value of the thermal gradient G_{S2} decreases with T_{10} and exhibits nonuniform behavior with respect to δ and T_{20}.

2.2 *Structure Formation*

Both amorphous and crystalline structures may arise in the first coating layer as well as in subsequent layers because of very high cooling velocities. In Ref 3, it was shown that the alloy phase of the WC-Co coating (on a low-carbon steel substrate) had a high glass forming ability and, therefore, a high probability of forming an amorphous structure. Coating characterization confirmed this probability (Ref 4, 9). The WC-Co coating structure on the aluminum alloy substrate is similar to that on the steel substrate (Ref 4, 9).

In general, the amorphous structure formed in the coating can be partially destroyed and transformed to a crystalline one by heat transfer from the impinging droplets when the temperature reaches 0.4 to 0.6 T_L, where T_L is the liquidus temperature of the coating alloy (Ref 10). As shown in Ref 1, these temperatures are attained in the coating process.

The calculated velocities of solidification and cooling and the thermal gradients at the liquidus and solidus can be used to determine the parameters of the fine crystalline (actually, nanocrystalline) structure of the layer, which is characterized by ξ, the size of crystals, and η, the distance between them. The following formulas for ξ and η are used (Ref 11):

$$\xi = a\, v_{S2}^{b}\, G_{S2}^{c} \qquad \text{(Eq 1)}$$

$$\eta = d \cdot v_{CS2}^{e} \qquad \text{(Eq 2)}$$

For calculating the coating layer structure, the parameters in Eq 1 and 2 were taken as $a = 4 \times 10^{-6}$, $b = -0.25$, $c = -0.5$, $d = 3.8$, and $e = -0.4$.

The ξ and η parameters increases away from the substrate-coating interface toward the interior of the layer.

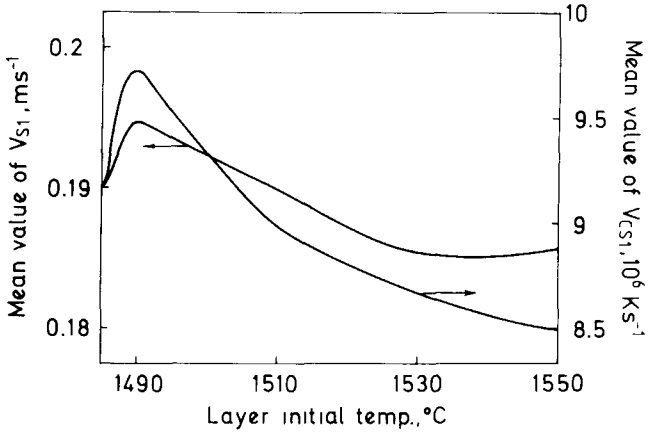

Fig. 9 Variations of mean values of solidification velocity, v_{S1}, and cooling velocity, v_{CS1}, with respect to layer initial temperature

The mean values of ξ increase with the layer thickness and diminish with its initial temperature (Fig. 4). Figure 5 shows that the mean values of η also grow with δ but vary nonuniformly with T_{20}. Both η and δ behave nonuniformly as the initial substrate temperature increases (Fig. 6).

The minimum values of ξ, corresponding to the finest crystalline structure, are expected when δ = 10 to 15 μm, T_{10} = 300 °C ,and T_{20} = 1540 °C. The densest structure should occur when η is at its minimum (when δ = 10 to 15 μm, T_{10} = 300 °C, and T_{20} = 1530 °C).

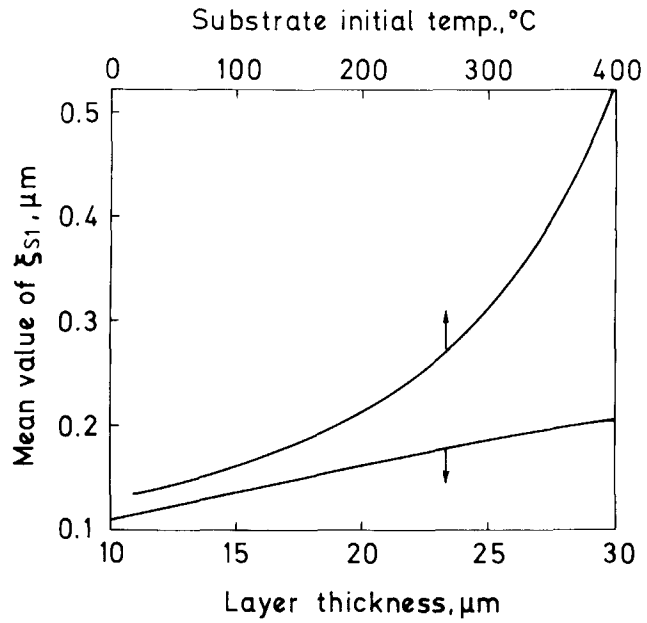

Fig. 10 Variations of mean values of crystal size, ξ_{S1}, with respect to layer thickness and substrate initial temperature

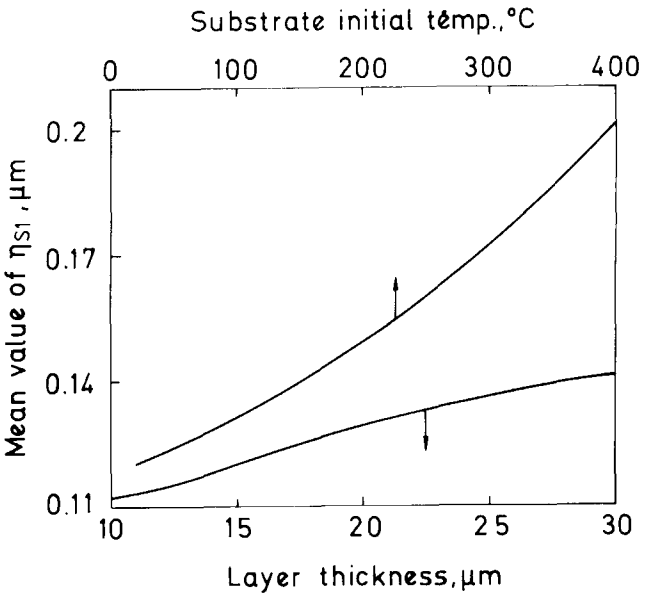

Fig. 11 Variations of mean values of intercrystalline distance, η_{S1}, with respect to layer thickness and substrate initial temperature

3. Substrate Interfacial Region

3.1 *Solidification Isotherms*

As heat is removed from the coating, the temperature in the substrate interfacial region increases and melting starts. The velocities of the liquidus and solidus surfaces during melting increase closer to the substrate.

When this melting process is completed and the maximum melting depth is achieved, solidification begins, and the liquidus and solidus velocities (v_{L1} and v_{S1}) increase closer to the substrate-coating interface. This increase is not as rapid as during melting because of the latent heat extraction.

During solidification, the thermal gradients at the liquidus (G_{L1}) and solidus (G_{S1}) diminish during melting and continue to decrease approaching the interface. The cooling rate increases in the interface direction, at first slowly and then more rapidly, because the extracted latent heat first exceeds the heat removed by the substrate, but later the latent heat extraction decreases. This change accelerates the solidus movement.

The mean solidification velocity, v_{S1} for the solidus diminishes with layer thickness and initial substrate temperature (Fig. 7).

Figure 8 shows that the mean cooling velocity, v_{CS1}, at the solidus also decreases with δ and T_{10}. The mean values of both v_{S1} and v_{CS1} vary nonuniformly with the initial layer temperature (Fig. 9). The mean values of the thermal gradient, G_{S1}, diminish when δ, T_{10} and T_{20} grow.

3.2 *Development of Crystalline Structure*

To determine the parameters of the crystalline structure in the substrate interfacial region, Eq 1 is used for ξ, and Eq 3 is used for η (Ref 1):

$$\eta = f \cdot G^{-g} \qquad \text{(Eq 3)}$$

The parameters are set to: $a = 2 \times 10^{-4}$, $b = -0.25$, and $c = -0.5$ in Eq 1, and $f = 8.8$ and $g = 0.275$ in Eq 3.

Calculations show that the crystal size, ξ, decreases toward the interior of the substrate. The intercrystalline distance, η, also diminishes in the same direction.

The mean crystal size, ξ, and the intercrystalline distance, η, calculated at the solidus isotherm (ξ_{S1}, η_{S1}) grow with the layer thickness and initial substrate temperature (Fig. 10, 11). When the initial layer temperature increases, the η_{S1} parameter increases, and ξ_{S1} varies nonuniformly (Fig. 12).

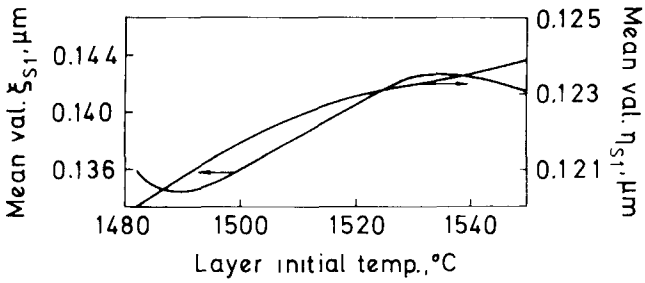

Fig. 12 Variations of mean values of crystal size, ξ_{S1}, and intercrystalline distance, η_{S1}, with respect to layer initial temperature

The minimum ξ corresponding to the finest crystalline structure in the substrate interfacial region occurs when $\delta = 10$ to 15 μm, $T_{10} = 20$ to 100 °C, and $T_{20} = 1485$ °C. The densest crystalline structure is expected when η is at its minimum, which takes place at the same δ, T_{10}, and T_{20}.

4. Subsequent Coating Layers

In Ref 1, it was shown that the solidification of the subsequent coating layers is slower than that of the first layer, mostly because thermal resistance is greater at the layer-layer interfaces where various defects (pores, inclusions, etc.) are concentrated. The ξ and η crystalline parameters are, therefore, increased. They vary with δ, T_{10}, and T_{20} in the same manner discussed for the first coating layer.

5. Comparison with the Experimental Data

HVOF spraying was carried out with the Plasma Technik AG PT100 system at the Centre of Thermal Spraying of the University of Barcelona. A commercial WC-(Co-40%W) powder was sprayed on to an Al-4%Cu alloy substrate.

The coating microstructure is similar to that described in Ref 9 while the microstructure in the substrate interfacial region significantly differs from that of the same coating on a steel substrate (Ref 12). They differ because of the differing thermal properties of the two substrate metals.

Four zones were identified in the substrate interfacial region. Zone 1 was in the substrate immediately adjacent to the interface and consisted of small equiaxed crystals with a diameter of about 0.25 μm (Fig. 13a). The width of this zone was about 10 μm. However, it was not uniform, and the zone boundary with the adjacent region was wavy. Zone 1 is the region where the al-

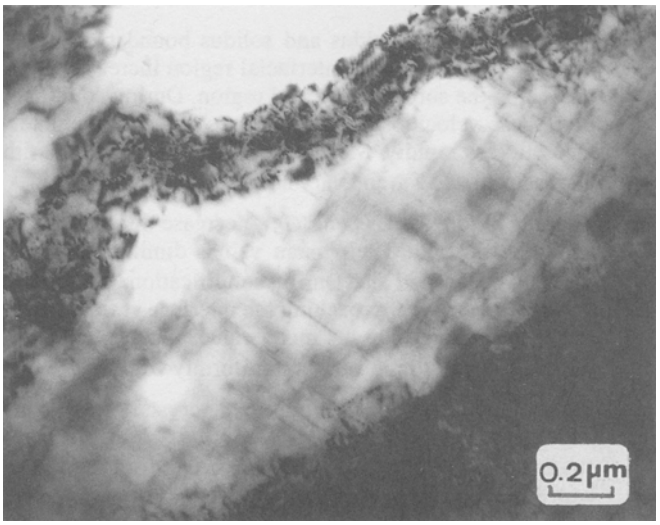

(a)

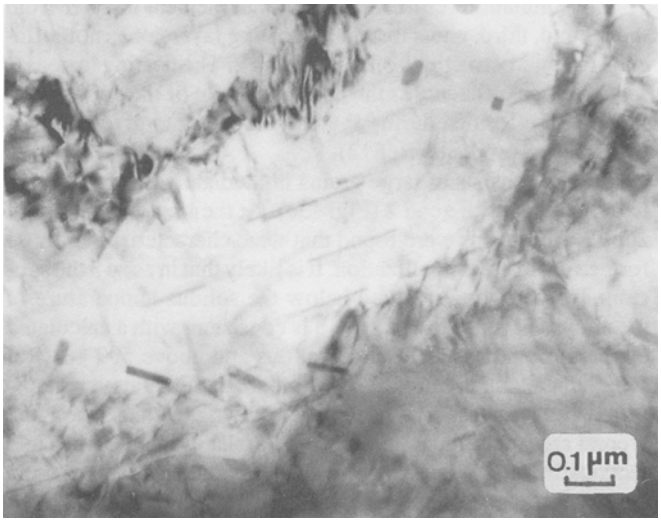

(b)

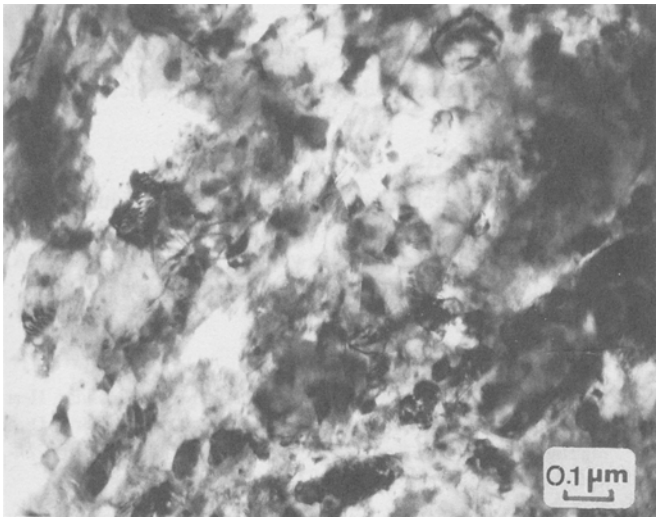

(c)

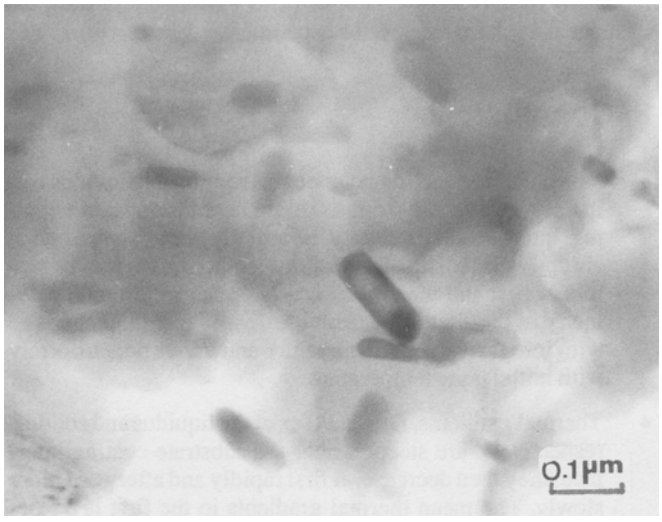

(d)

Fig. 13 Transmission electron microscopy (TEM) micrographs of zones (a) 1, (b) 2, (c) 3, and (d) 4 in the aluminum alloy substrate

loy has been molten. It is consistent with the modelling results, which show that after the arrival of the first splat, the temperature rises rapidly to about 1200 °C in 10^{-7} s and then decreases so that after about 10^{-4} s it falls to about the aluminum melting point. The calculations also show that the width of zone 1 is about 8 to 14 μm depending on the spraying conditions (Ref 1). According to the modelling results, the mean crystal size in zone 1 developed during solidification of the fully molten alloy (determined using the parameters of the liquidus isotherm) is about 0.2 to 0.3 μm. Thus the theoretical results agree with the experimental data.

Immediately below zone 1 is a narrow layer about 5 μm wide (zone 2). It consists of fine grains having diameters of about 50 nm (Fig. 13b). The structure of this zone is consistent with partial melting of the alloy to give solid and liquid phases (mushy state). The calculations show that in this zone, the maximum substrate temperature is between the liquidus and solidus of the alloy. They predict the width of this zone to be 4 to 6 μm (Ref 1, 12).

The simulation results also show that the heat transfer from the second, third, and subsequent coating layers does not influence the microstructures of zones 1 and 2. The heating in zone 2 seems to be sufficient for the decomposition of the copper-rich liquid phase formed during the initial heating to give eutectic-like reaction products (Ref 12).

Zone 3 consists of large grains immediately adjacent to the lower boundary of zone 2 (Fig. 13c). At the lower boundary of zone 3, fine grains were found that were characteristic of those formed during recrystallization. It is likely that in zone 3 the substrate temperature remained below the solidus temperature of the alloy. The structure of zone 3 is consistent with a calculated temperature profile below the solidus and above 500 °C (Ref 12). Such a temperature range would lead to partial recrystallization and recovery. The heat pulses coming to zone 3 from the second and subsequent layers would assist in the recovery and recrystallization processes. Thus, the theoretical results again agree with the experimental data.

Zone 4 of the microstructure was almost identical to the original substrate structure (Fig. 13d), as confirmed by the results of the modelling of the substrate thermal history (Ref 1, 12). Thus, the theoretical results agree with the experimental data.

6. Conclusions

- When the first coating layer begins to cool, the liquidus isotherm moves away from its origin near the substrate-coating interface. Its velocity is initially very high; then it abruptly diminishes. The solidus isotherm also moves rapidly at first and then more slowly. Mean solidification velocity in the first layer decreases with layer thickness and with initial substrate temperature and varies nonuniformly with initial layer temperature.
- Thermal gradients, G_{L2} and G_{S2}, at the liquidus and solidus, respectively, are steepest near the substrate-coating interface; they then decrease, at first rapidly and afterward more slowly. The mean thermal gradients in the first layer decrease with increasing initial substrate temperature and vary nonuniformly with layer thickness and initial layer temperature.
- Cooling velocities corresponding to the isotherms of liquidus and solidus in the coating first layer sharply decrease near the interface and then vary more slowly. Their mean values decrease with the layer thickness and vary nonuniformly with the initial layer and substrate temperatures.
- At the very high cooling velocities found in the coating layers, both amorphous and very fine crystalline structures can be formed. The solidifying alloy is very likely to be a glass forming system. The amorphous structure developed can be partially destroyed and transformed to crystalline structure by heat transfer from the impinging droplets.
- Crystal size and intercrystalline distance increase from the interface to the layer inner part. The mean values of ξ increase with δ and decrease with increasing T_{20}. The mean values of η also grow with δ and vary nonuniformly with T_{20}. Both these parameters vary nonuniformly with T_{10}. The finest and densest crystalline structure can be expected when $\delta = 10$ to 15 μm, $T = 300$ °C, and $T_{20} =$ 1530 to 1540 °C.
- Velocities of the liquidus and solidus boundaries during melting in the substrate interfacial region increase on approaching the substrate internal region. During solidification, these velocities also increase approaching the interface but less rapidly. Mean velocities, v_{S1}, diminish with increasing δ and T_{10} and vary nonuniformly with T_{20}.
- Thermal gradients, G_{L1} and G_{S1}, decrease during melting and solidification. Their mean values diminish with increasing δ, T_{10}, and T_{20}. During solidification, the cooling velocity increases approaching the interface at first slowly and then more rapidly. Its mean values decrease with increasing δ and T_{10} and vary nonuniformly with T_{20}.
- In the substrate interfacial region, the crystal size and the intercrystalline distance decrease approaching the substrate internal region. The mean values of ξ_{S1} and η_{S1} grow with δ and T_{10}. When T_{20} increases, η_{S1} increases while ξ_{S1} varies nonuniformly. The finest and densest crystalline structure in the substrate interfacial region is likely to be formed when $\delta = 10$ to 15 μm, $T_{10} = 20$ to 100 °C, and $T =$ 1485 °C.
- Theoretical results agree well with the experimental data, and the developed model can be used for prediction.

Acknowledgments

The authors are grateful to the Generalitat de Catalunya (GC) for the financial support received with project GRQ93-1017. V.V. Sobolev thanks GC for his visiting professor grant. J.A. Calero is also thankful to GC for the concession of a F.I. grant.

References

1. V.V. Sobolev, J.M. Guilemany, J.A. Calero, and F.J. Villuendas, Heat Transfer Between WC-Co Coating and Aluminum Alloy Substrate During High Velocity Oxy-Fuel (HVOF) Spraying, *J. Therm. Spray Technol.*, Vol 4(4), 1995, p 408-414
2. C.C. Berndt, W. Brindley, A.N. Goland, H. Herman, D.L. Houck, K. Jones, R.A. Miller, R. Neiser, W. Riggs, S. Sampath, M. Smith, and P. Spanne, Current Problems in Plasma Spray Processing, *J. Thermal Spray Technol.*, Vol 1 (No. 4), 1992, p 341-356

3. V.V. Sobolev, J.M. Guilemany, and J.A. Calero, Substrate-Coating Thermal Interaction During High Velocity Oxy-Fuel (HVOF) Spraying. Part 2. Structure Formation, *Mater. Sci. Technol.*, Vol 11, No. 10, 1995

4. J.M. Guilemany, V.V. Sobolev, J. Nutting, Z. Dong, and J.A. Calero, Thermal Interaction Between WC-Co Coating and Steel Substrate in Process of HVOF Spraying, *Scr. Metall. Mater.*, Vol 31 (No. 7), 1994, p 915-920

5. V.V. Sobolev, J.M. Guilemany, J.R. Miguel, and J.A. Calero, Investigation of Coating Structure Development in Process of High Velocity Oxy-Fuel (HVOF) Spraying of WC-Ni Powder Particles, Surf. Coat. Technol., in press, 1995

6. V.V. Sobolev, J.M. Guilemany, and J.A. Calero, Substrate-Coating Thermal Interaction During High Velocity Oxy-Fuel (HVOF) Spraying. Part 1. Heat Transfer Processes, *Mater. Sci. Technol.*, Vol 11, No. 8, 1995, p 810-819

7. V.V. Sobolev and J.M. Guilemany, Investigation of Coating Porosity Formation During High Velocity Oxy-Fuel (HVOF) Spraying, *Mater. Lett.*, Vol 18, 1994, p 304-308

8. V.V. Sobolev and J.M. Guilemany, Analysis of Coating Gas Porosity Development During Thermal Spraying, *Surf. Coat. Technol.*, Vol 70, 1994, p 57-68

9. J. Nutting, J.M. Guilemany, and Z. Dong, The Substrate-Coating Interface Structure of WC-Co HVOF Sprayed Coating on to Low Alloy Steel, *Mater. Sci. Technol.*, Vol 11, No. 9, 1995

10. F.E. Lubrosky, Ed., *Amorphous Metallic Alloys*, Butterworths, London, 1983, p 144-168

11. W. Kurz and D.J. Fisher, *Fundamentals of Solidification*, Trans. Tech., Aedermannsdorf, 1984, p 65-97

12. J.M. Guilemany, J. Nutting, Z. Dong, and J.M. de Paco, The Influence of WC-Co HVOF Thermal Spraying on the Microstructure of an Aluminum Alloy Substrate, *Scr. Metall. Mater.*, Vol 33, No. 7, 1995, p 1055-1062